



HAL
open science

Luminosity Sensing Application of Negative Group Delay Predictor

Blaise Ravelo, Mathieu Guerin, Lala Rajaoarisoa, Wenceslas Rahajandraibe

► **To cite this version:**

Blaise Ravelo, Mathieu Guerin, Lala Rajaoarisoa, Wenceslas Rahajandraibe. Luminosity Sensing Application of Negative Group Delay Predictor. IEEE Transactions on Industrial Electronics, 2023, pp.1-11. 10.1109/TIE.2023.3321988 . hal-04440919

HAL Id: hal-04440919

<https://hal.science/hal-04440919>

Submitted on 6 Feb 2024

HAL is a multi-disciplinary open access archive for the deposit and dissemination of scientific research documents, whether they are published or not. The documents may come from teaching and research institutions in France or abroad, or from public or private research centers.

L'archive ouverte pluridisciplinaire **HAL**, est destinée au dépôt et à la diffusion de documents scientifiques de niveau recherche, publiés ou non, émanant des établissements d'enseignement et de recherche français ou étrangers, des laboratoires publics ou privés.

Luminosity Sensing Application of Negative Group Delay Predictor

Blaise Ravelo, *Senior Member, IEEE*, Mathieu Guerin, *Member, IEEE*, Lala Rajaoarisoa, *Member, IEEE*, and Wenceslas Rahajandraibe, *Member, IEEE*

Abstract—This article features on original application of negative group delay (NGD) predictor for the luminosity pre-detection. The low-pass (LP) type NGD prediction theory is established based on the time-advance consideration. The analytical design condition in function of expected prediction performance is formulated. The LP-NGD predictor is studied and characterized by using ramp signal input. The validity of the LP-NGD digital predictor with STM32® microcontroller implementation is verified by trapezoidal test signals having different rise/fall times and arbitrary waveform signal. Furthermore, excellent test result of real application is presented by using NLS-4942 luminosity photoresistor. An LP-NGD prediction demonstrator is designed and implemented with different time-advances (-30 ms, -50 ms and -70 ms). The calculated and experimented results in good agreement show negative skew transient responses. The NGD predictor is potentially useful for industrial applications as object detection, car safety and smart building comfortability control system.

Index Terms—Light sensor, Negative group delay (NGD) predictor, Infinite impulse response (IIR) design, prediction technique, NGD digital circuit, skew prediction.

I. INTRODUCTION

THE LUMINOSITY is one of the most important physical parameters of today engineering for industrial environment monitoring and living comfortability. The luminosity is naturally used for different systems of irradiation detection [1-3]. For example, the luminosity was widely explored in the process of weather prediction [1]. High luminosity colliders were employed for tracking with diamond radiation [2]. More importantly, an industrial application of luminosity constitutes a key element of light intensity prediction for automatic smart room [3]. The luminosity sensing allows environment monitoring as range sensing and object detection, for vehicle active safety [4]. Luminosity sensors and occlusion processing were developed for reliable vehicle detection [5]. An innovative light sensor was introduced for indoor positioning and navigation [6]. Industrial technology achievement was reported based on constant innovation of sensor system [7-9]. More

recently, integrated circuit [7-8] and neural network occupancy estimation via Bayes filter [9] luminosity sensors were proposed. The progress of luminosity sensor design enables to perform object detection [10-12]. However, certain detection systems may meet anomaly in real-time operation because of distribution time delay [12] and also for remote control [13]. The reduction of communication delay impact [14] on detection transmission signal remains a challenging effort for the industrial system design engineers. To overcome this challenge, a luminosity sensing-based pre-detection technique is proposed in this article by using negative group delay (NGD) electronic circuits [15-18]. It was emphasized that the NGD function is susceptible to reduce delay [15-16], to operate with time-advance behavior [17] and to predict arbitrary waveform medical and industrial signals [18].

Indeed, the NGD signature is defined by the uncommon ability to propagate sensor signals in time-advance [17-29]. Despite the counterintuitive aspect, the NGD function does not contradict the causality [19-20]. Nevertheless, the uncommon NGD circuit design remains misunderstood and unfamiliar to most of industrial electronic engineer designers. The NGD function was initially studied in theory and by experiment with low frequency (LF) analog circuits composed of lumped elements as resistor, inductor, capacitor and operational amplifier [19-23]. Because of circuit topology diversity, the NGD function interpretation was an open question to most of electronic and industrial design engineers. A fundamental theory inspired from filter was initiated [24]. The concept of low-pass (LP) type NGD behavior [24-25] was defined when the electronic circuit group delay (GD) is negative in very LF. But so far, the LP-NGD circuit usefulness to develop prediction method can be increased with the range of time-advance. For the cases of several minutes or hours prediction as the weather [1] or rainfall [26-27] data, the NGD analog circuits do not work due to the resistor, inductor and capacitor component value limits [19-25]. To overcome these limitations, NGD digital circuits operating with some minutes and even some hours were recently designed, implemented and experimented [28-29]. The NGD digital circuit theory was introduced by considered

Manuscript received xxx xx, 2023; revised xxx xx, 2023; accepted xxx xx, 2023. Date of publication xxx xx, 2023. (Corresponding author: Dr. Blaise Ravelo)

Blaise Ravelo is with the Nanjing University of Information Science & Technology (NUIST), Nanjing 210044, Jiangsu, China (E-mail: blaise.ravelo@yahoo.fr).

Mathieu Guerin, and Wenceslas Rahajandraibe are with the Aix-Marseille University, CNRS, University of Toulon, IM2NP UMR7334, 13007 Marseille, France (E-mail: {mathieu.guerin, wenceslas.rahajandraibe}@im2np.fr).

Lala Rajaoarisoa is with IMT Nord Europe, University of Lille, Centre for Digital Systems, F-59000 Lille, France (E-mail: lala.rajaoarisoa@imt-nord-europe.fr).

infinite impulse response (IIR) function [30-31]. So far, few research works are available in the literature about the NGD digital circuit application.

The LP-NGD predictor theory, design, implementation and test is originally investigated in the present article for pre-detection of luminosity operating with negative skew generation. The article is organized in four sections. First, Section II focuses on the industrial challenge of luminosity pre-detection test scenario. Then, the LP-NGD predictor theory is established in Section III by considering ramp signals and showing negative skew responses. Section IV discusses on the proof-of-concept (POC), prototyping and experimentation with NSL-4942 luminosity sensor [32] by implementing the NGD function on STM32® microcontroller unit (MCU) [33]. Last, Section V is the conclusion.

II. SCENARIO OF LUMINOSITY PRE-DETECTION TEST

The scenario and characterization of luminosity pre-detection using photoresistor is introduced in this section.

A. Description of Luminosity Test Experimental Setup

The proposed test consists in examining the luminosity pre-detection scenario by predicting the environmental object mechanical state. The pre-detection experiment was performed

by placing the luminosity sensor in the shelf drawer as depicted by Fig. 1(a). The experimentation test setup includes the monitoring PC driving an STM32® MCU manufactured by STMicroelectronics® by Fig. 1(a). As seen in Fig. 1(b), the tested sensor is TO-8 NSL-4942 photocells operating as photoresistor manufactured by SILONEX® Inc. [32]. The test setup synoptic is explained by Fig. 1(c). The block diagram is constituted by the driver and data storage PC, the calculator board using STM32® MCU and the photocells integrating its appropriate conditioning circuit. The predictor synoptic diagram works with the conversion of luminosity by the photocells into output voltage signal V_{sensor} which is injected into the MCU which is connected to the sensor conditioning circuit supplied by $V_{dd}=5\text{ V}_{DC}$.

B. Luminosity Pre-detection Problem Formulation

The problem formulation is inspired from industrial scenario with mechanical control via luminosity detection and light control of security [2-6]. Fig. 2 depicts the representation of the experiment integrating the predictor. The synoptic diagram introduced by Fig. 1(a) operates with two main states:

- “Open-position” corresponds to the drawer in open position. The photocells are exposed to the room light.
- “Close-position” corresponds to the drawer in closed position and photocells placed in the dark.

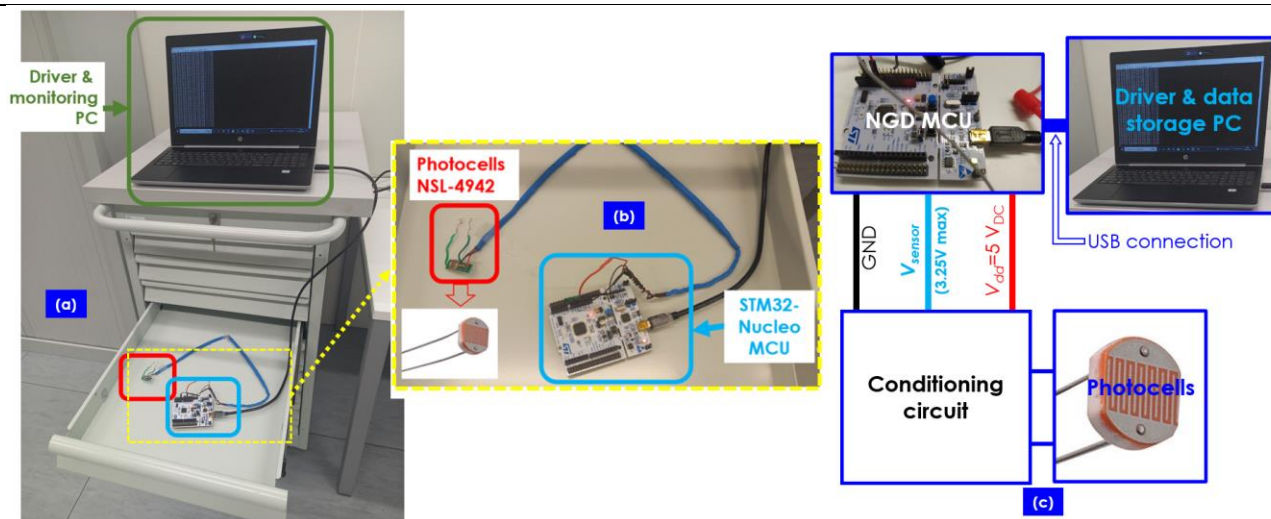


Fig. 1. Luminosity pre-detection (a) experimental setup, (b) photocells and STM32® MCU photographs, and (c) synoptic diagram.

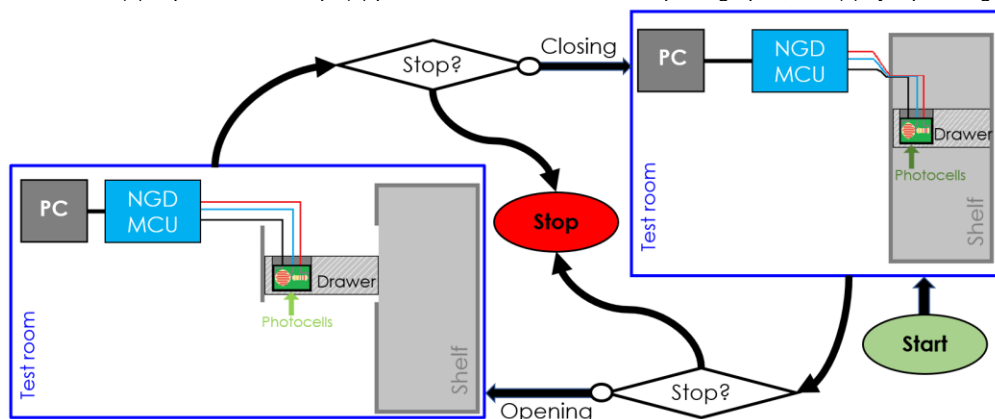


Fig. 2. Illustrative scenario of luminosity pre-detection with open/close-state drawer experiment.

As illustrated by the workflow shown by Fig. 2, the overall system operates as follows:

- First, we assume that we have light detection when V_{sensor} is equal to the threshold.
- The main objective of the study is to anticipate the switching or transition position of the drawer by means of the detected signal states.
- We can have either “high voltage state x_H ” or “low voltage state x_L ” defined by:

$$V_{sensor} = \begin{cases} x_L = 0 & \text{if } V_{out} \leq 0.2V_{max} \\ x_H = V_{max} & \text{if } V_{out} \geq 0.8V_{max} \end{cases}. \quad (1)$$

- To avoid the fault detection caused by the undesirable noise, a denoising filter can be integrated to the sensor conditioning circuit output.

C. Photoresistor Characterization Technique

The NSL-4942 photoresistor operates with CdS resistance range available in hermetic package operating between -60°C to 75°C [32]. The sensor presents the specifications of typical light resistance $R_{typical}$ @ 100 ftc minimum resistance in the dark R_{DARK} , maximum test voltage V_t , and maximum power dissipation P_{max} @ 25°C addressed by Table I.

TABLE I
EMPLOYED PHOTORESISTOR SPECIFICATIONS

Parameters	$R_{typical}$	R_{DARK}	V_t	P_{max}
Value	30 Ω	50 k Ω	80 V	250

The photoresistor illuminated by a lamp connected to multimeter is characterized by the light test synoptic proposed by Fig. 3(a). The sensor environment luminosity is measured with a luxmeter.

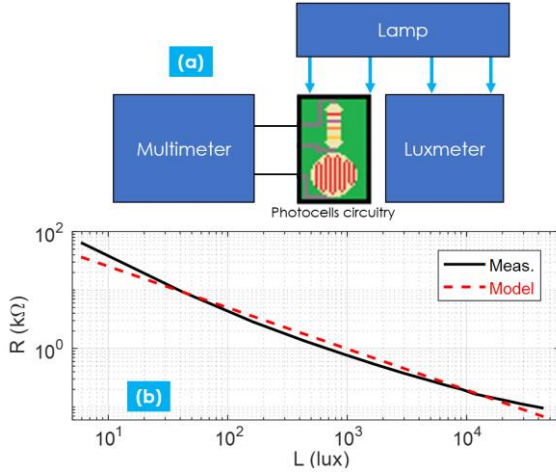


Fig. 3. NSL-4942 sensor (a) test synoptic and (b) light-resistance characteristic.

The NSL-4942 sensor characterization was performed following the steps: (i) the light from the projector is gradually sent to the sensor, (ii) the resistance is measured with the multimeter and the quantity of light at the same time and (iii) thus, the light-resistance logarithmic characteristic shown by Fig. 3(b) is plotted in black solid curve. The empirical model between the sensor resistance R in Ω and light L varied in interval [6 lux, 45 klux] plotted in red dashed curve of Fig. 3(b) is approximated by:

$$R \approx 128719L^{-0.705}. \quad (2)$$

The NGD-predictor theory illustrating how to generate the negative skew is described in the next section.

III. THEORIZATION OF LP-NGD PREDICTOR WITH ANALYSIS OF SLEW-RATE RESPONSE

This section describes the LP-NGD predictor theory. After frequency domain analysis, the negative skew effect is explained by the transient response of input ramp deterministic signal. The prediction theory is established from LP-NGD digital circuit in function of targeted time-advance $t_n < 0$.

A. Frequency Domain Analysis of LP-NGD Predictor Ramp Response

We recall that the LP-NGD function is characterized by its temporal signature related to its time-advance t_n and NGD cut-off frequency f_n . By denoting s the Laplace variable, we can demonstrate that the canonical form of 1st order LP-NGD analog TF:

$$N(s) = \frac{1 + t_1 s}{1 + t_2 s} \quad (3)$$

where:

$$\begin{cases} t_1 = \frac{t_n}{\gamma - 1} > 0 \\ t_2 = \frac{t_n \gamma}{\gamma - 1} > 0 \end{cases} \quad (4)$$

with positive parameter $\gamma < 1$ (meaning while $t_1 > t_2$) related to the NGD cut-off frequency:

$$f_n = \frac{\gamma - 1}{2\pi t_n \sqrt{\gamma}}. \quad (5)$$

By taking $s = j\omega$, the frequency domain analysis is based on the transmittance:

$$N(j\omega) = \frac{1 + j\omega t_1}{1 + j\omega t_2} \quad (6)$$

which has magnitude $N(\omega) = |N(j\omega)|$ and GD:

$$GD(\omega) = \frac{-\partial \arg[N(j\omega)]}{\partial \omega} \quad (7)$$

with:

$$GD(\omega = \omega_n = 2\pi f_n) = 0. \quad (8)$$

At very low frequency $\omega \approx 0$, we have:

$$\begin{cases} N(\omega \approx 0) = 1 \\ GD(\omega \approx 0) = t_n \end{cases}. \quad (9)$$

B. Negative Skew Analytical Demonstration with LP-NGD Predictor Ramp Response

The present NGD prediction study is essentially based on time-dependent input signal x assumed as a ramp waveform:

$$x(t) = \gamma \cdot t \cdot \Gamma(t) \quad (10)$$

with slope λ in the time interval $[0, t_{max}]$ and Γ is the Heaviside function by considering the rest initial state $x(t=0)=0$.

In this case, the input amplitude is:

$$x_{max} = \lambda \cdot t_{max}. \quad (11)$$

The LP-NGD symbolic output $Y(s) = N(s)X(s)$ is expressed by

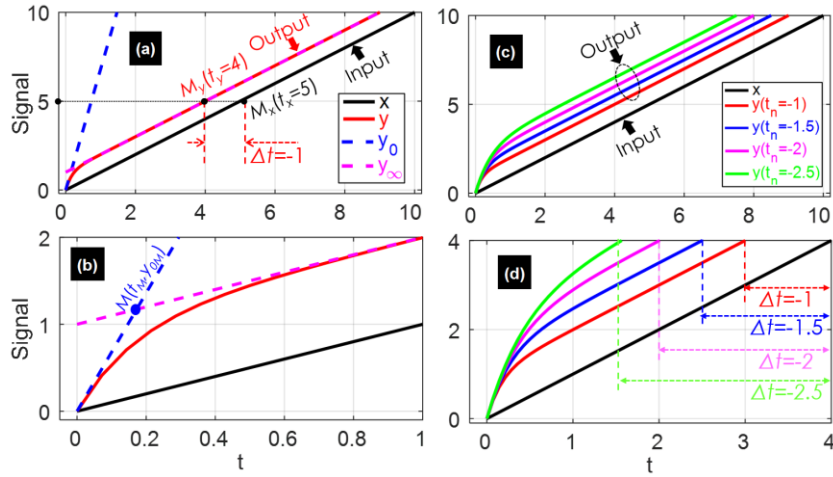


Fig. 4. Plots of (y, y_0, y_∞) for (a) $t \in [0, 10]$ and (b) $t \in [0, 1]$ and of $(y_{t_n=-1}, y_{t_n=-1.5}, y_{t_n=-2}, y_{t_n=-2.5})$ for $t \in$ (c) $[0, 10]$ and (d) $[1, 4]$ compared to x .

$$Y(s) = \frac{\lambda(1+t_1s)X(s)}{s^2(1+t_2s)}. \quad (12)$$

By means of inverse Laplace transform, we theoretically have:

$$y(t) = \lambda[t + (t_1 - t_2)(1 - e^{-t/t_2})] \cdot \Gamma(t). \quad (13)$$

It can be emphasized from this equation that:

- When $t < t_2$, at the beginning $t \rightarrow 0$, we have the asymptotic $e^{-t/t_2} \rightarrow 1 - t/t_2$ which implies:

$$y_0(t) = \lambda \left(1 - \frac{t_n}{t_2} \right) t. \quad (14)$$

- When $t \rightarrow \infty$ ($t > t_2$) knowing that $t_1 - t_2 = -t_n$, we have the asymptotic behavior $e^{-t/t_2} \rightarrow 0$ which implies the output expressed by:

$$y_\infty(t) = \lambda(t - t_n) \cdot \Gamma(t) \Rightarrow y_\infty(t) = x(t - t_n). \quad (15)$$

As $t_n < 0$, the present instant value of $y(t)$ at $t = \tau > t_2$, is the predicted value of $x(\tau - t_n)$ at future instant $t = \tau - t_n$. This finding confirms that we have a time-advance effect.

- When $t = t_2$, we have:

$$\begin{cases} y_0(t_2) = y_\infty(t) = \lambda \cdot t_1 \\ y(t_2) = \gamma[t_1 - e^{-1}(t_1 - t_2)] \end{cases}. \quad (16)$$

Fig. 4(a) represents the calculated responses (y, y_0, y_∞) from equations (13), (14) and (15) with targeted time-advance $t_n = -1$. The transient diagrams show the comparison of outputs and input x with $x_{\max} = 1$ for $t \in [1, 10]$. Fig. 4(b) plots the asymptotes y_0 and y_∞ which intersect at $M(t_m = t_2 \approx 0.172)$, and explains that the predicted responses present absolute error $|y(t) - y_\infty(t)|$ lower than 5% when $t > 0.6$. The prediction effect is obviously highlighted by points $M_x(t_x = 5)$ and $M_y(t_y = 4)$ for threshold $x_T = y_T = x_{\max}/2 = 5$ with the evaluated time-advance $\Delta t = t_y - t_x = -1$. Fig. 4(c) explains the behavior of predicted responses $(y_{m=-1}, y_{m=-1.5}, y_{m=-2}, y_{m=-2.5})$ with respect to the different objectives t_n . Fig. 4(d) shows a good agreement between the assessed time-advances $\Delta t = \{-2.5, -2, -1.5, -1\}$ and the objectives t_n .

C. Analysis of LP-NGD Predictor Ramp Response

According to the signal processing theory, the frequency spectrum of input denoted by $X(\omega) = |X(j\omega)|$, calculated by the Fourier transform, is given by:

$$X(\omega) = \frac{\lambda}{\omega^2}. \quad (17)$$

To avoid output significant distortion with respect to the LP-NGD TF, the input $x(t)$ should have limited bandwidth [24-25, 28-29, 31]. The input spectrum must be delimited by the NGD bandwidth $\omega_{\max} = 2\pi f_n$. Therefore, we have the prediction efficiency under the condition:

$$\frac{X(\omega \leq \omega_{\max})}{x_{\max}} \leq \varepsilon \quad (18)$$

with $\varepsilon < -20$ dB. By taking into account previous relations (17) and (18), it can be established that the time-advance must respect the following condition in function of input ramp parameters:

$$\frac{\lambda}{\omega_{\max}^2} \leq \varepsilon \Rightarrow \frac{x_{\max}}{4\pi^2 t_{\max}^2 f_n^2} \leq \varepsilon \Rightarrow |t_n| \leq \frac{\sqrt{(1-\gamma)t_{\max}\varepsilon}}{\gamma\sqrt{x_{\max}}}. \quad (19)$$

Knowing the design condition, the LP-NGD theory based IIR TF is investigated in the next subsection.

D. LP-NGD Predictor Difference Equation

The discretization of the input $x(t)$ is performed by assuming the sampling period T_s . The discrete samples are denoted by $x_k = x(t) = x(t_k)$ with positive integer index:

$$k = \left\lceil \frac{t}{T_s} \right\rceil \quad (20)$$

with $\lceil \cdot \rceil$ the ceil function. The sampled discrete time is given by $t_k = k \cdot T_s$. We assume that the discrete impulse response n_k associated to the output $y_k = n_k(x_k)$ is expressed by the first order difference equation:

$$y_{k+1} = b_2 x_{k+1} + b_1 x_k + b_0 y_k \quad (21)$$

where b_0 , b_1 and b_2 are real coefficients. We point out that the LP-NGD prediction design method developed in the present research work is derived from the analysis of the previous difference equation. Fig. 5 represents the digital structure diagram of LP-NGD function governed by equation (21). According to the proposed difference equation, we have the symbolic relation:

- The z-transform of equation (21) implies the expressions of input $X(z)$ and output $Y(z)=N(z)X(z)$. The corresponding IIR TF is expressed as:

$$N(z) = \frac{b_1 + b_0 z}{1 - b_0 z}. \quad (22)$$

- The LP-NGD time-advance signature can be graphically understood with diagram of Fig. 5. Hence, the time-advance between input x_k and output y_k for every sequence k of MCU is graphically represented by time shift Δt .

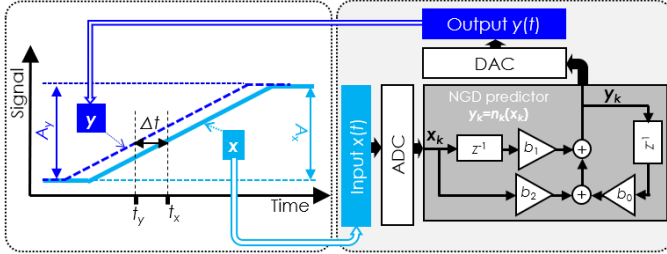


Fig. 5. Structural diagram highlighting the NGD operation principle.

To perform the LP-NGD prediction characterization of TF n_k , we need to evaluate the time difference related to chosen threshold x_T according to relation:

$$\begin{cases} x_T = x(t_x) = y(t_y) \\ \Delta t = t_y - t_x \end{cases}. \quad (23)$$

In addition, the difference between the input and LP-NGD predictor output amplitudes can be evaluated from A_x and A_y .

- To reach relative error precision on the time-advance signature $t_n = \Delta t \pm T_s$ better than 25%, we must respect condition:

$$|t_n| \geq 4T_s. \quad (24)$$

The methodology of LP-NGD predictor synthesis, design and implementation is described in the following subsection.

E. LP-NGD Predictor Synthesis, Design and Implementation Methodology

The present subsection formulates the synthesis method and implementation of LP-NGD predictor introduced by equation (21). The synthesis aims to generate signal prediction in function of the targeted time-advance t_n ideally characterized by transient input and output relationship $y(t) \approx x(t + t_n)$. For this reason, the LP-NGD predictor synthesis consists in determining difference equation (21) in function of the targeted time-advance $t_n < 0$. It is clear that instead of positive delay effect usually for classical electronic circuit, we realize the transient signal prediction represented by the output y . Consequently, the design of the LP-NGD predictor is carried out by the calculation of parameter coefficients representing the IIR numerical function.

The LP-NGD predictor synthesis formulas are established by solving the equation related to the GD at low frequencies. It yields the synthesis formulas of difference equation two coefficients:

$$b_0 = \frac{at_n}{(a-1)T_s + at_n} \quad (25)$$

$$b_1 = \frac{at_n}{(1-a)T_s - at_n} \quad (26)$$

$$b_2 = \frac{a[(a-1)T_s + t_n]}{(a-1)T_s + at_n}. \quad (27)$$

By taking into account the design condition of previous subsection, the implementation methodology of the developed LP-NGD predictor is summarized in the actions of five main steps as indicated by the workflow of Fig. 6. In brief, the initial step is the specifications of the luminosity test signals as the amplitude, rise/fall time and sampling period. The desired time-advance t_n and the NGD cut-off frequency must be defined. The predictor difference equation parameters are calculated from formulas (25), (26) and (27). The POC design and implementation are using the coefficients and the coding in the considered digital platform. Then, like all electronic circuit design, the proposed methodology must be ended by an experimental validation step.

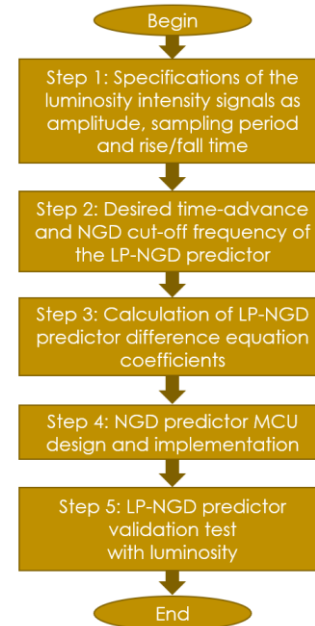


Fig. 6. Workflow of LP-NGD predictor design and implementation.

The following section discusses on experimental validation of design and implementation methodology the LP-NGD predictor.

IV. EXPERIMENTAL INVESTIGATION OF LUMINOSITY PRE-DETECTION

This section validates the previous LP-NGD predictor theory with two main demonstrators showing the negative skew due to the time-advance effect. The POC design was performed following the methodology described by Fig. 6. The first experimentation was carried out with periodical voltage signals. Then, the luminosity pre-detection results from the second demonstrator which uses luminosity sensor NSL-4942 photocells introduced by the illustrative setup diagram shown by Fig. 1(a) is also examined.

A. LP-NGD Light Predictor Design, Prototype and Test

The LP-NGD predictor was designed by calculating the coefficients given by formulas (25), (26) and (27) with $T_s = 10$

ms with different targeted time-advances t_n . The LP-NGD predictor was implemented on STM32L476RG 64-pin MCU used in [28-29,31] in C-language program pseudo-code written in Algorithm 1. As depicted by the synoptic diagram introduced by Fig. 1(c), the considered MCU platform board is fed by $V_{dd}=5 V_{DC}$ power from USB connector operating with 12-bits precision. The test signal dynamic range is defined between $V_{min}=0 V$ to $V_{max}=3 V$ and quantum resolution equal to $\Delta V=0.8 mV$. The test program was executed by applying analog input voltage $V_{sensor}(t)$ injected on by pin15/PA1. The input signal is converted into digital data $x_0=x(t)$. Figs. 7 highlight the experimental setup diagram and photograph of LP-NGD predictor test board. In this study case, the input test signal x is provided by the generator source. We can see that the input and output signals x and y are visualized simultaneously by the oscilloscope.

Algorithm 1. Luminosity predictor implemented pseudo code

```

1: float b0 = xxx; float b1 = xxx; float b2 = xxx;
2: float x_1 = 0; float x_0 = 0; float y_1 = 0; float y_0 = 0;
3: return float Process(float input)
4: {
5: // Update internally stored output at t[k]
6: y_0 = y_1;
7: // Update internally stored input at t[k]
8: x_0 = x_1;
9: // Update internally stored input at t[k+1]
10: x_1 = input;
11: // Compute output
12: y_1 = b2*x_1+b1*x_0+b0*y_0;
13: return y_1;
14: }
    
```

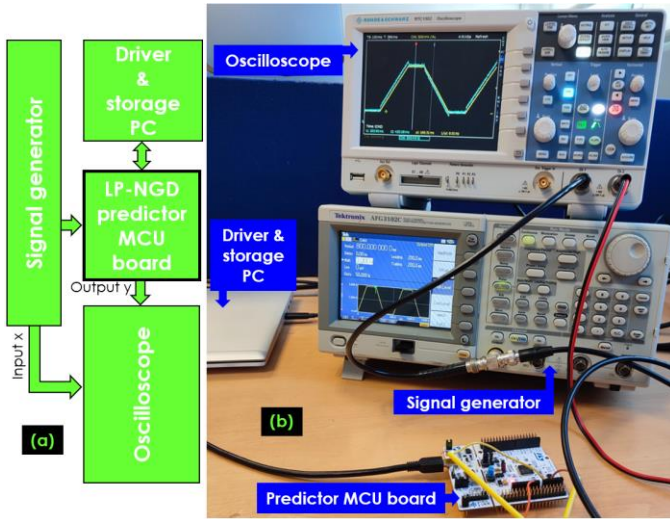


Fig. 7. (a) Illustrative and (b) photograph LP-NGD predictor test setup.

TABLE II
TEST EQUIPMENT SPECIFICATIONS

Description	Reference	Parameter	Value
Arbitrary function generator	Tektronix AFG3102C Dual Channel	Sampling rate	1 GS/s
		Bandwidth	100 MHz
Digital oscilloscope	RTC1002 ROHDE&SCHWARZ®	Resolution	12.5 mV
		Sampling rate	4 GSa/s
		Bandwidth	1 GHz
		Channels	2

The obtained data results are recorded in CSV-format and replotted in MATLAB® environment. The test equipment specifications are addressed by Table II. During the validation

test, the MCU configuration including the input and output signal interactions with the microprocessor is carried out by using the STM32CubeIDE software installed on the driver PC. The transient results representing the LP-NGD predictor response are discussed in the following paragraph.

The obtained validation results of the LP-NGD predictor POC and prototype is characterized with input signal transient voltage generator in the following subsection.

B. LP-NGD Predictor Transient Test Characterization

The present subsection investigates on the characterization results of the LP-NGD predictor prototype. First, we consider essentially the input voltage behaving as periodic trapezoidal test signal. Then, the predictability of arbitrary waveform and trapezoidal signal will also be discussed.

1) Prediction Result of Trapezoidal Waveform Signal

The input ramp is controlled by changing the periods $T_{k=1,2,3}$ and rise/fall times $t_{r,k=1,2,3}$ of different test signals $signal_{k=1,2,3}(T_k, t_{r,k})$. The LP-NGD predictor coefficients are indicated by Table III. The coefficients were calculated from the test signal $_{k=1,2,3}$ parameters by fixing $a=0.147$.

TABLE III
LP-NGD PREDICTOR COEFFICIENTS

Parameter	Value		
T	$T_1=0.65 s$	$T_2=0.8 s$	$T_3=1.6 s$
t_r	$t_{r1}=0.1 s$	$t_{r2}=0.2 s$	$t_{r3}=0.3 s$
t_n	-30 ms	-50 ms	-70 ms
f_n	133.3 Hz	76.9 Hz	40 Hz
b_0	0.0182	0.0311	0.0582
b_1	-0.7546	-1.2907	-2.4127
b_2	1.7363	2.2595	3.3545

Figs. 8 and Figs. 9 show the comparison between the calculated and measured results of LP-NGD predictor prototype specified in Table III. The total duration of the considered test signal is $T=4 s$.

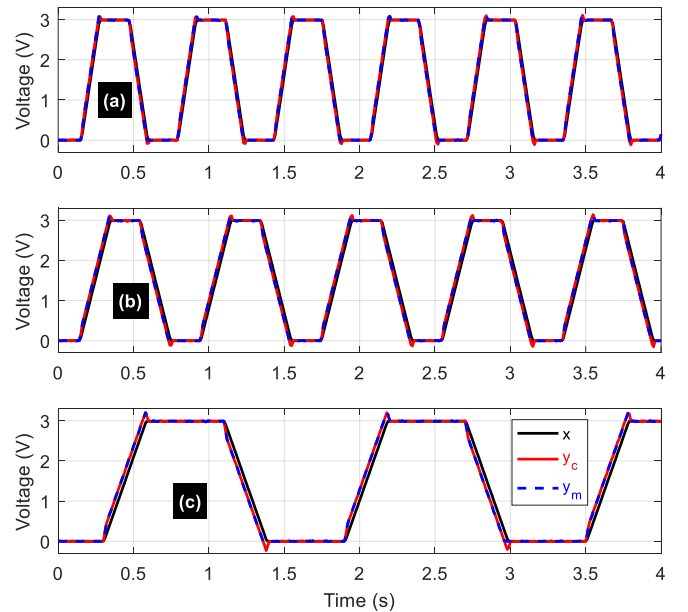


Fig. 8. Calculated and measured LP-NGD predictor responses for (a) signal₁, (b) signal₂ and (c) signal₃.

Fig. 8(a), Fig. 8(b) and Fig. 8(c) highlight a very good agreement between the input x (black solid lines), calculated y_c (red solid lines) and measured y_m (blue dashed lines) transient output results of signal₁, signal₂ and signal₃, respectively. As

seen in the zoom plots of Fig. 9(a), Fig. 9(b) and Fig. 9(c), the negative skew effect is successfully validated for signal₁, signal₂ and signal₃, respectively. It can be observed that the leading- and tailing- edge of LP-NGD predictor outputs are clearly anticipated with respect to the targeted time-advances. For the present study case of trapezoidal input test, the LP-NGD validation is also performed by the comparison of:

- Input-output gain related to high- and low-level states, x_H and x_L , respectively, defined by:

$$\rho = \frac{|y_H - y_L|}{|x_H - x_L|} \quad (28)$$

- And the input-output cross correlation coefficient defined by MATLAB® function “*corrcoef*” written as:

$$\zeta(x, y) = \text{corrcoef}[x(t), y(t)]. \quad (29)$$

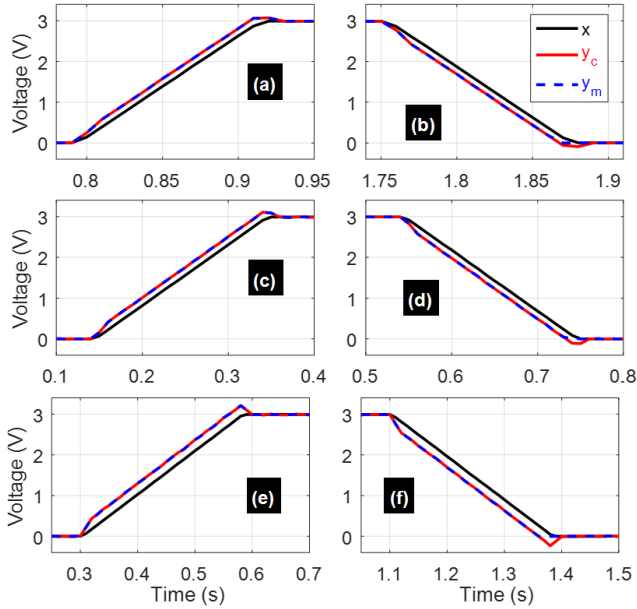


Fig. 9. Zoom in plots of calculated and measured LP-NGD predictor responses: signal₁ in the time-interval (a) $TI_a=[0.78 \text{ s}, 0.95 \text{ s}]$ and (b) $TI_b=[1.74 \text{ s}, 1.91 \text{ s}]$, signal₂ in (c) $TI_c=[0.1 \text{ s}, 0.4 \text{ s}]$ and (d) $TI_d=[0.5 \text{ s}, 0.8 \text{ s}]$, and signal₃ (e) $TI_e=[0.25 \text{ s}, 0.7 \text{ s}]$ and (f) $TI_f=[1.05 \text{ s}, 1.5 \text{ s}]$.

Table IV summarizes the transient characterization specifications of the LP-NGD predictor. We emphasize that the time-advance absolute value assessed from results of Figs. 8 increase with the ideal targeted time-advance t_n . The design and implementation feasibility of the unfamiliar predictor is confirmed by the good correlation of assessed time-advance.

TABLE IV

COMPARISON OF CALCULATED AND MEASURED LP-NGD PREDICTOR TRANSIENT CHARACTERISTICS

Input signal		Signal ₁	Signal ₂	Signal ₃
Δt_{rise}	Calculated	-8.2 ms	-12.6 ms	-25.8 ms
	Measured	-8 ms	-12 ms	-25 ms
Δt_{fall}	Calculated	-8.15 ms	-12.5 ms	-25.7 ms
	Measured	-8 ms	-12 ms	-25 ms
ρ	Calculated	1.001	1.001	1.001
	Measured	1.061	1.063	1.076
ζ	Calculated	99.9%	99.98%	99.9%
	Measured	99.88%	99.95%	99.91%

2) LP-NGD Prediction Result of Arbitrary Waveform Input Signal

In spite of the validation of ramp input prediction which represents the main behavior of luminosity sensor signals, we

may ask also about the general cases of test signal predictability. For this reason, the present further study of LP-NGD predictor by considering the case of non-trapezoidal signal is proposed. In this study case, the input signal was considered as a completely arbitrary waveform. Then, the desired time-advance was fixed to $t_n=-70 \text{ ms}$. The LP-NGD-prototype was designed and implemented under the same process as the previous paragraph because we use the same digital board platform. The input signal was randomly defined from MATLAB® environment. The test configuration was carried out by recording the input data in CSV-format and imported to the generator source following the test setup shown by Figs. 7. The transient test of the LP-NGD prototype was performed by simultaneously visualizing input x and output y . As result, Fig. 10(a) confirm the input arbitrary waveform signal predictability showing the desired time-advance.

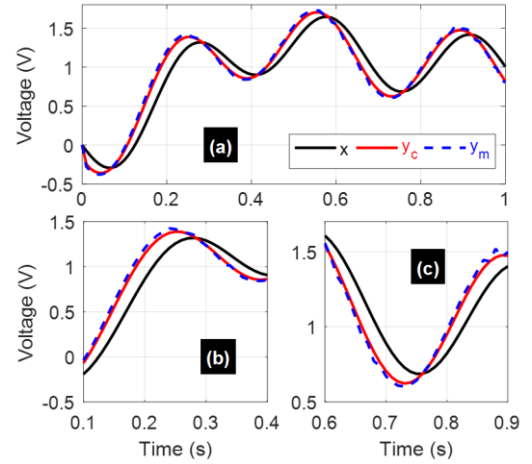


Fig. 10. Calculated and measured LP-NGD predictor arbitrary waveform signal responses for in time-intervals (a) TI_1 , (b) TI_2 and (c) TI_3 .

The calculated and experimented transient responses are visualized in the time-interval $TI_1=[0,1 \text{ s}]$. For the better visibility of the signal prediction, zooms in plot of x and y in time-intervals $TI_2=[0.1 \text{ s}, 0.4 \text{ s}]$ and $TI_3=[0.6 \text{ s}, 0.9 \text{ s}]$ are proposed by Fig. 10(b) and Fig. 10(c), respectively. As illustrated by Figs. 10, by referring to non-trapezoidal input x , an excellent correlation between the simulated and experimented predicted signals y_c and y_m is observed with the expected time-advance equal to -70 ms . In addition to the generator source test, real-time experimentation with photoresistor sensor signals is reported by the following subsection.

C. Luminosity Sensor Test Validation with LP-NGD Predictor

The feasibility study of LP-NGD prediction with industrial luminosity sensor signal is reported in this subsection. In this study case, the practical test was performed following the workflow explained by the scenario introduced by Fig. 2. The open/close drawer test was experimentally carried out with maximal duration $t_{max}=28 \text{ s}$ by fixing $a=0.147$. LP-NGD predictor prototype with coefficients addressed by Table V was designed for $t_n=-75 \text{ ms}$ targeted time-advance. The photoresistor including the voltage divider conditioning circuit constituted by resistors $R_p=27 \text{ k}\Omega$ and $R(t)$ was interconnected to the MCU as illustrated by Fig. 11.

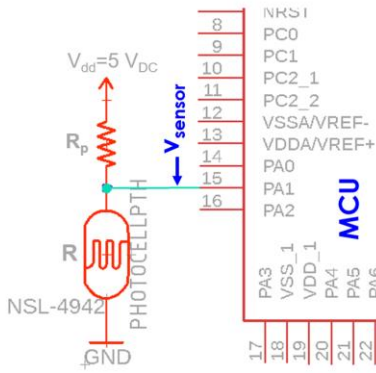


Fig. 11. Photoresistor-MCU interconnection.

 TABLE V
 TESTED LP-NGD PREDICTOR COEFFICIENTS

Parameters	T_s	f_n	b_0	b_1	b_2
Value	965 μ s	13.33 Hz	0.6576	-27.2621	27.6044

The performed experimentation is based on the comparison of calculated and measured outputs corresponding to input voltage $v_{sensor}(t)=x(t)$ across the NSL-4942 photocells and the ground (GND). The time-dependent photocells resistance is given by the voltage divider principle:

$$R(t) = \frac{R_p V_{dd}}{V_{dd} - x(t)}. \quad (30)$$

The calculated and measured time-dependent voltage and photoresistor resistance obtained from the open/close drawer test are plotted in Figs. 12(a) and Fig. 12(b), respectively. To highlight the negative skew behavior, the transient results are plotted in arbitrary chosen time-intervals $TI_1=[0, 6.2 \text{ s}]$ and $TI_2=[22.5 \text{ s}, 27.5 \text{ s}]$ of Fig. 12(c) and Fig. 12(d), respectively. Despite the output signal overshoot and under-shoot of about 11%, the calculated and measured results are in good correlation. Table VI summarizes the assessed LP-NGD characteristics.

 TABLE VI
 CALCULATED AND MEASURED LP-NGD PREDICTOR CHARACTERISTICS

Parameters	Δt_{rise}	Δt_{fall}	ρ	r
Calculation	-48.5 ms	-22.6 ms	1.02	97.4%
Measurement	-50 ms	-23 ms	1.019	98.6%

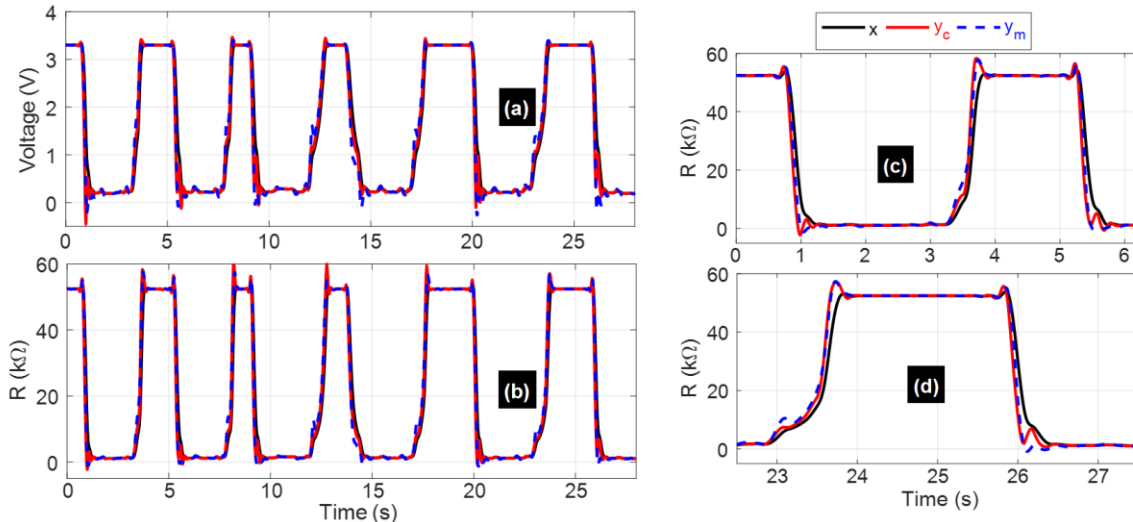


Fig. 12. LP-NGD predictor real test results of luminosity sensor test shown by Fig. 1(a) representing the transient (a) voltage and (b) resistance. Zoom in time-dependent resistance plots in the time intervals (c) [0, 6.2 s] and (d) [22.5 s, 27.5 s].

This comparative test result confirms the luminosity pre-detection feasibility showing negative skew. We emphasize that in this case, the cross correlation between the input-output sensed signal is 98.6%. The rise and fall mean time-advances were assessed.

D. Potential Applications of Luminosity NGD Predictor

The developed luminosity pre-detection NGD method has potential industrial applications such as:

- (i) Consumer electronics application [35]: One of NGD predictor applications is the remote-control devices that operate on infrared light and using photodiodes. Light sensors are used for wide range of functions on smartphones, tablets and many electronic devices. They operate with motion and automatic brightness sensors found in smartphones use light detectors like photo-transistors.
- (ii) Security device application [36-37]: In the security application, the luminosity detection is commonly used to process shipping cargoes to ensure boxes are properly sealed or not. Several types of motion sensors using light sensors detect the change in light exposure. Photodiodes are also used in smoke detectors found in offices, airports, trains, etc;
- (iii) Car device application [38-40]: Light sensors or detectors are used in automobiles to detect surrounding ambient light. These detectors turn on automatically the lights of the automobile when it is dark. Nowadays, light sensors are used in several car models to ensure driving and parking safety.

Some particular reasons illustrating why the LP-NGD prediction can be less efficient in some real-case of application is discussed in the comparative study of following subsection.

E. Strength and Weakness of the Developed LP-NGD Predictor

Despite the previous validation, one may wonder about the LP-NGD predictor method limit compared to the existing ones. However, based on the authors knowledge, most of research work available literature on light sensor [2-11] are focused on design, modeling and test but not prediction.

Therefore, we consider some popular prediction method for more general cases to state the effectiveness of the studied LP-NGD predictor. Table VII recapitulated the main particularity allowing to state the limitation of the LP-NGD predictor.

TABLE VII
RECAPITULATION OF LP-NGD PREDICTOR STRENGTH AND LIMIT

Reference	Prediction time-advance	Signal waveform	Amplitude dynamics	x-y correlation
[1]	hour and day scale and time-advance delimited by the data processing duration	Depending on weather variability	No limit	Good
[26]		Any		
[27]		Any		
This work	From milli-second to several month	Any	Delimited by ADC & DAC resolution	Sensitive to noise effect & signal bandwidth

The developed NGD prediction method is beneficial for automatic detection with different ranges of time-advance with any signal waveform. It is worth to note that the NGD digital predictor is particularly advantageous for slow signals. But the analog circuit based NGD predictor can easily be designed and applied to fast signals with nano- and micro-seconds time-advances as introduced in [16,17,18,19,20][23,24,25]. However, the NGD prediction digital circuit is not efficient for large amplitude dynamics, noisy and very wideband signals. For this reason, the noise influence study according to the application environment constitutes the main perspective of our research work study.

V. CONCLUSION

An innovative study of LP-NGD predictor application for luminosity pre-detection is developed. The LP-NGD theorization is elaborated by analog and digital TF analyses. The theoretical expression demonstrates how the LP-NGD predictor generates the negative skew by means of input ramp signal. The methodology of POC synthesis, design and implementation of LP-NGD predictor from the targeted time-advances is introduced. The feasibility of the developed LP-NGD predictor theory is studied. During the experimental test of two practical study cases, the prototype was implemented on STM32® MCU digital platform. First, signal generator source-based experimentations were performed with trapezoidal signals having different periods and rise/fall times. Substantially, prediction of luminosity signals with pre-detection and negative skew according to the targeted time-advance is approved by MATLAB® calculation and experimentation. The other validation study is based on industrial test scenario. An original setup based on open/closer drawer real test by using NSL-4942 photoresistor [33] was considered to generate the light sensor signal. The obtained results confirm the predictability of light sensor signal with -75 ms time-advance. The feasibility of drawer state prediction was observed by using the LP-NGD pre-detector. Some potential applications of the developed in LP-NGD predictor is

discussed. In the future, the LP-NGD predictor is expected to be used in the societal consumer electronic devices and industrial system notably on monitoring method of automatic production line with light prediction [35-40].

REFERENCES

- [1] A. Fouilloy, C. Voyant, G. Notton, F. Motte, C. Paoli, M.-L. Nivet, E. Guillot and J.-L. Duchaud, "Solar irradiation prediction with machine learning: Forecasting models selection method depending on weather variability," *Energy*, vol. 165, Part A, pp. 620-629, Dec. 2018.
- [2] S. Schnetzer et al., "Tracking with CVD diamond radiation sensors at high luminosity colliders," *IEEE Tran. Nuclear Science*, vol. 46, no. 3, pp. 193-200, Jun. 1999.
- [3] Y. -W. Bai and Y. -T. Ku, "Automatic room light intensity detection and control using a microprocessor and light sensors," *IEEE Tran. Consumer Electronics*, vol. 54, no. 3, pp. 1173-1176, Aug. 2008.
- [4] W. Deng, J. Dai, Q. Zhao, B. Litkouhi, N. Moshchuk and R. Nisonger, "Modeling of range sensing and object detection, for vehicle active safety," *Proc. 2009 12th Int. IEEE Conf. on Intelligent Transportation Systems*, St. Louis, MO, USA, 2009, pp. 1-6.
- [5] A. Faro, D. Giordano and C. Spampinato, "Adaptive Background Modeling Integrated With Luminosity Sensors and Occlusion Processing for Reliable Vehicle Detection," *IEEE Tran. Intelligent Transportation Systems*, vol. 12, no. 4, pp. 1398-1412, Dec. 2011.
- [6] A. D. Cheok and L. Yue, "A Novel Light-Sensor-Based Information Transmission System for Indoor Positioning and Navigation," *IEEE Tran. Instrumentation and Measurement*, vol. 60, no. 1, pp. 290-299, Jan. 2011.
- [7] E. Chalfin, "A Precision Light Sensor Integrated Circuit," *IEEE Tran. Consumer Electronics*, vol. CE-28, no. 3, pp. 337-345, Aug. 1982.
- [8] W. -J. Chiang, C. -J. Lin, Y. -C. King, A. -T. Cho, C. -T. Peng and W. -M. Huang, "Integrated Ambient Light Sensor With Nanocrystalline Silicon on a Low-Temperature Polysilicon Display Panel," *IEEE Tran. Electron Devices*, vol. 56, no. 4, pp. 578-586, Apr. 2009.
- [9] Z. Chen, Y. Yang, C. Jiang, J. Hao and L. Zhang, "Light Sensor Based Occupancy Estimation via Bayes Filter With Neural Networks," *IEEE Tran. Industrial Electronics*, vol. 67, no. 7, pp. 5787-5797, Jul. 2020.
- [10] X. Liang, J. Zhang, L. Zhuo, Y. Li and Q. Tian, "Small Object Detection in Unmanned Aerial Vehicle Images Using Feature Fusion and Scaling-Based Single Shot Detector With Spatial Context Analysis," *IEEE Tran. Circuits and Systems for Video Technology*, vol. 30, no. 6, pp. 1758-1770, Jun. 2020.
- [11] Q. Yu, B. Wang and Y. Su, "Object Detection-Tracking Algorithm for Unmanned Surface Vehicles Based on a Radar-Photoelectric System," *IEEE Access*, vol. 9, pp. 57529-57541, 2021.
- [12] P.-Y. Chen, S. Yang and J. A. McCann, "Distributed Real-Time Anomaly Detection in Networked Industrial Sensing Systems," *IEEE Tran. Industrial Electronics*, vol. 62, no. 6, pp. 3832-3842, June 2015.
- [13] A. Maiti, A. A. Kist and A. D. Maxwell, "Real-Time Remote Access Laboratory With Distributed and Modular Design," *IEEE Tran. Industrial Electronics*, vol. 62, no. 6, pp. 3607-3618, June 2015.
- [14] S. Liu, X. Wang and P. X. Liu, "Impact of Communication Delays on Secondary Frequency Control in an Islanded Microgrid," *IEEE Tran. Industrial Electronics*, vol. 62, no. 4, pp. 2021-2031, Apr. 2015.
- [15] D. Solli, R. Y. Chiao and J. M. Hickmann, "Superluminal effects and negative group delays in electronics, and their applications," *Phys. Rev. E*, vol. 66 (056601), pp. 1-12, 2002.
- [16] C. Hymel, R. A. Stubbers and M. E. Brandt, "Temporally Advanced Signal Detection: A Review of the Technology and Potential Applications," *IEEE CAS Magazine*, vol. 11, no. 3, pp. 10-25, 2011.
- [17] B. Ravelo, S. Lall ch re, A. Thakur, A. Saini and P. Thakur, "Theory and circuit modelling of baseband and modulated signal delay compensations with low- and band-pass NGD effects," *Int. J. Electron. Commun.*, vol. 70, no. 9, Sept. 2016, pp. 1122-1127.
- [18] H. U. Voss, "Signal prediction by anticipatory relaxation dynamics," *Phys. Rev. E*, Vol. 93, No. 3, (030201R), pp. 1-5, 2016.
- [19] M. W. Mitchell and R. Y. Chiao, "Causality and Negative Group-delays in a Simple Bandpass Amplifier," *Am. J. Phys.*, vol. 66, 1998, pp. 14-19.
- [20] M. W. Mitchell and R. Y. Chiao, "Negative Group-delay and 'Fronts' in a Causal Systems: An Experiment with Very Low Frequency Bandpass Amplifiers," *Phys. Lett. A*, vol. 230, Jun. 1997, pp. 133-138.

- [21] T. Nakanishi, K. Sugiyama and M. Kitano, "Demonstration of Negative Group-delays in a Simple Electronic Circuit," *Am. J. Phys.*, vol. 70, no. 11, 2002, pp. 1117-1121.
- [22] M. Kitano, T. Nakanishi and K. Sugiyama, "Negative Group-delay and Superluminal Propagation: An Electronic Circuit Approach," *IEEE J. Sel. Top. in Quantum Electron.*, vol. 9, no. 1, Feb. 2003, pp. 43-51.
- [23] J. N. Munday and R. H. Henderson, "Superluminal Time Advance of a Complex Audio Signal," *Appl. Phys. Lett.*, vol. 85, July 2004, pp. 503-504.
- [24] B. Ravelo, "Similitude between the NGD function and filter gain behaviours," *Int. J. Circ. Theor. Appl.*, vol. 42, no. 10, Oct. 2014, pp. 1016-1032.
- [25] B. Ravelo, "First-order low-pass negative group delay passive topology," *Electronics Letters*, vol. 52, no. 2, Jan. 2016, pp. 124-126.
- [26] L. Gao, F. Wei, Z. Yan, J. Ma and J. Xia, "A study of objective prediction for summer precipitation patterns over eastern China based on a multinomial logistic regression model," *Atmosphere*, vol. 10, no. 4 (213), pp. 1-18, Apr. 2019.
- [27] S. Manandhar, S. Dev, Y. H. Lee, Y. S. Meng and S. Winkler, "A data-driven approach for accurate rainfall prediction," *IEEE Tran. Geoscience and Remote Sensing*, vol. 57, no. 11, pp. 9323-9331, Nov. 2019.
- [28] B. Ravelo, M. Guerin, W. Rahajandraibe, V. Gies, L. Rajaoarisoa and S. Lalléchére, "Low-Pass NGD Numerical Function and STM32 MCU Emulation Test," *IEEE Tran. Industrial Electronics*, vol. 39, no. 8, Aug. 2022, pp. 8346-8355.
- [29] B. Ravelo, M. Guerin, J. Frnda, L. Rajaoarisoa and W. Rahajandraibe, "Thermal Wave Variation Anticipation under Minute Scale Time-Advance with Low-Pass NGD Digital Circuit," *IEEE Access*, vol. 10, Dec. 2022.
- [30] B. Ravelo, "Elementary NGD IIR/FIR Systems," *Int. J. Signal Processing Systems (IJSPS)*, vol. 2, no. 2, Dec. 2014, pp. 132-138.
- [31] B. Ravelo, M. Guerin, W. Rahajandraibe and L. Rajaoarisoa, "All-Pass NGD FIR Original Study for Sensor Failure Detection Application," *IEEE Tran. Industrial Electronics*, vol. 70, no. 9, Sept. 2023, pp. 9561-9571.
- [32] TO-8 Photocells, NSL-4942, SILONEX, Available [Online], Accessed May 14 2023, <https://www.digchip.com/datasheets/parts/datasheet/443/NSL-4942.php>.
- [33] ST, STM32L476xx, Datasheet-Production Data, pp. 1-270, June 2019.
- [34] D. -B. Ma and M. -F. Qu, "Research on on-line Monitoring Method of Automatic Production Line based on Industrial Internet of Things," *2020 IEEE International Conference on Industrial Application of Artificial Intelligence (IAAI)*, Harbin, China, 2020, pp. 492-496.
- [35] Available [Online], Accessed May 14 2023, <https://www.keyence.fr/products/sensor/photoelectric/lr-z/>.
- [36] Available [Online], Accessed May 14 2023, <https://www.baumer.com/fr/fr/aperçu-du-produits/detection-dobjets/barrieres-photoelectriques-et-detecteurs-reflex/laser/c/14177>.
- [37] Available [Online], Accessed May 14 2023, <https://www.ifm.com/fr/fr/shared/technologies/magic-cube/detecteurs-laser>.
- [38] Available [Online], Accessed May 14 2023, <https://www.hella.com/techworld/fr/Technique/Electricite-et-electronique/Capteur-pluie-luminosite-defectueux-42078/>.
- [39] Available [Online], Accessed May 14 2023, <https://www.ecinews.fr/fr/capteur-de-lumiere-pour-phares-automobiles-a-laser/>.
- [40] Available [Online], Accessed May 14 2023, <https://vipress.net/photodiodes-pin-a-4-segments-pour-lautomobile/>.



Prof. Dr. Blaise RAVELO (M'09) is currently University Full Professor at NUIST, Nanjing, China. His research interest is on Multiphysics modelling, Kron's method, RF/electronics engineering, EMC/SI/PI of PCBs, and pioneer of the negative group delay (NGD) theory, engineering and application for data prediction. With international partners, he is actively involved and contributes on several international research projects. He is member of IET Electronics Letters editorial board as circuit & system

subject editor. He supervised 10 PhD students. He is member of scientific technical committee of Advanced Electromagnetic Symposium (AES) 2013-

2023 and IMOC2021. He is ranked in Top 2% world's scientists based on years (2020-2022) by Stanford University, US. He has Google scholar h-index(2023)=29 and i10-index(2023)=94. He is member of research groups: IEEE, URSI, GDR Ondes, Radio Society and (co) authors of more than 400 scientific research papers in new technologies published in int. conf. and journals.



Dr. Mathieu GUERIN obtained an engineering degree in Microelectronics and Telecommunications from Polytech Marseille in 2010 and at the same time a Research Master in Integrated Circuits Design from the University of Aix-Marseille. He obtained his PhD degree from the same institution in 2013. He worked as technical leader of the analog and radio-frequency design team of IDEMIA-StarChip for five years and designed chips embedded in SIM cards and contactless bank cards with biometric recognition. He joined Aix-Marseille University as an Assistant Professor in 2020 and joined the CCSI team of the IM2NP laboratory. His research focuses mainly on the design and synthesis of circuits in digital electronics. He is also working on methods of modeling and characterizing circuits in analog electronics.



Dr. Lala Rajaoarisoa is currently an Assistant Professor at the Institut Mines-Télécom Lille Douai. He received his M.Sc. degree and PhD in Automatic and Computer Sciences, both at the University of Aix-Marseille, France in 2005 and 2009. His research interests are the development of data-driven tools and methods for the observation and control of large-scale distributed systems. Develop predictive models and controllers to assess system behavior and optimize its performance. This development includes the analysis of

intrinsic properties such as stability, observability, identifiability and controllability. He is involved in research activities dedicated to the optimization of energy efficiency of building systems and the control and management of hydraulic systems with more than 80 papers published in refereed journals and conferences. He regularly participates and contributes on several international projects (ANR, FUI, and INTERREG) and was the supervisor of more than of 15 PhD students, postdocs, research engineers and Master internships.



Prof. Dr. Wenceslas RAHAJANDRAIBE is currently full professor at the University of Aix-Marseille. He received the B. Sc. degree in electrical engineering from Nice Sophia-Antipolis University, France, in 1996 and the M. Sc. (with distinction) in electrical engineering from the University of Montpellier, Science department, France, in 1998. Since 1998, he joined the microelectronics department of Informatics, Robotics and Microelectronics Laboratory of Montpellier and received the Ph. D. on

Microelectronics from the University of Montpellier. Since 2003, he joined the microelectronic department of Materials, Microelectronics and Nanoscience Laboratory of Provence in Marseille, France where he was an Associate Professor. Since 2014, he is Professor at Aix Marseille University where he heads the Integrated Circuit Design group of this laboratory. He is regularly involved to participate and to lead national and international research projects (ANR, H2020, FP7 KIC-InnoEnergy...). His research interests involve AMS and RF circuit design from transistor to architectural level. His present research activity is focused on ultralow power circuit design for smart sensor interface and embedded electronic in bioelectronic and e-health applications, wireless systems, design technique and architecture for multi-standard transceiver. He is an expert for the ANR, the French Agency for Research. He has served on program committees of IEEE NEWCAS and ICECS. He has been and is a reviewer of contributions submitted to several IEEE conferences and journals such as ISCAS, NEWCAS, MWSCAS, ESSCIRC, ESSDERC, RFIC, and IEEE Transactions on Circuits and Systems I and II, IET Electronics Letters.